CAPN2-responsive mesoporous silica nanoparticles: a promising nanocarrier for targeted therapy of pancreatic cancer

Slapak, E.J.; el Mandili, M.; Brink, M.S. ten; Kros, A.; Bijlsma, M.F.; Spek, C.A.

Original Articles

CAPN2-responsive mesoporous silica nanoparticles: A promising nanocarrier for targeted therapy of pancreatic cancer

Etienne J. Slapak [a,b,*], Mouad el Mandili [a], Marieke S. Ten Brink [a], Alexander Kros [c], Maarten F. Bijlsma [a,b,1], C. Arnold Spek [a,b,1]

[a] Amsterdam UMC Location University of Amsterdam, Center of Experimental and Molecular Medicine, Meibergdreef 9, Amsterdam, the Netherlands
[b] Cancer Center Amsterdam, Cancer Biology, Amsterdam, the Netherlands
[c] Department of Supramolecular & Biomaterials Chemistry, Leiden Institute of Chemistry, Leiden University, Leiden, the Netherlands

ARTICLE INFO

ABSTRACT

Pancreatic adenocarcinoma (PDAC) is highly resistant to conventional chemotherapeutic interventions, resulting in exceptionally low survival rates. The limited efficacy can in part be attributed to dose limitations and treatment cessation urged by toxicity of currently used chemotherapy. The advent of targeted delivery strategies has kindled hope for circumventing off-target toxicity. We have previously reported a PDAC-specific mesoporous silica nanoparticle (MSN) containing a protease linker responsive to ADAM9, a PDAC-enriched extracellularly deposited protease. Upon loading with paclitaxel these ADAM9-MSNs reduced side effects both *in vitro* and *in vivo*, however, disappointing antitumor efficacy was observed *in vivo*. Here, we propose that an efficient uptake of MSNs by tumor cells might underlie the lack of antitumor efficacy of MSNs functionalized with linker responsive to *extracellular* proteases. Harnessing this premise to improve antitumor efficacy, we performed an *in silico* analysis to identify PDAC-enriched *intracellular* proteases. We report the identification of BACE2, CAPN2 and DPP3 as PDAC enriched intracellular proteases, and report the synthesis of BACE2-, CAPN2- and DPP3-responsive MSNs. Extensive preclinical assessments revealed that paclitaxel-loaded CAPN2- and DPP3-MSNs exhibit high PDAC specificity *in vitro* as opposed to free paclitaxel. The administration of paclitaxel-loaded CAPN2- and DPP3-MSNs *in vivo* confirmed the reduction of leukopenia and induced no organ damage. Promisingly, in two mouse models CAPN2-MSNs reduced tumor growth at least as efficiently as free paclitaxel. Taken together, our results pose CAPN2-MSNs as a promising nanocarrier for the targeted delivery of chemotherapeutics in PDAC.

1. Introduction

Pancreatic cancer (PDAC) stands out as the most lethal among common cancers, with a dismal 5-year overall survival rate of less than 9% [1,2]. While substantial strides have been made in the broader field of cancer treatment, PDAC continues to lag behind, with surgical resection standing as the lone potentially curative option. In the context of non-resectable PDAC, the prevailing first-line treatment options involve the systemic administration of gemcitabine combined with nab-paclitaxel, and combination therapy of fluorouracil, leucovorin, oxaliplatin, and irinotecan (FOLFIRINOX). However, these strategies face challenges due to dose-limiting toxicities, leading to treatment cessation in a substantial proportion of patients, ranging from 60% to 70% [3]. Noteworthy side effects manifest as nausea, fatigue, diarrhea, neutropenia, and neuropathy.

Nanocarriers have emerged as a promising solution to mitigate systemic toxicity of chemotherapeutics while enhancing their therapeutic precision [4]. These nanocarriers offer the prospect of targeted delivery of chemotherapeutic agents to malignant cells while sparing non-tumorous counterparts. Among the different nanocarriers, mesoporous silica nanoparticles (MSNs) have shown significant potential [5]. MSNs are notable for their porous architecture, allowing a high drug-loading capacity. In addition, MSNs are biocompatible and both

Abbreviations

ABHD17C	Abhydrolase Domain Containing 17C, Depalmitoylase
ADAM9	A disintegrin and metalloprotease domain 9
ADAM9-MSNs	ADAM9-responsive mesoporous silica nanoparticles
ALAT	Alanine aminotransferase
ASAT	Aspartate aminotransferase
BACE2	Beta-Secretase 2
BACE2-MSN	BACE2-responsive mesoporous silica nanoparticles
BMDL	Bone Marrow-Derived Leukocytes
CAPN2	Calpain 2
CAPN2-MSN	CAPN2-responsive mesoporous silica nanoparticles
CDK4	Cyclin-dependent kinase 4
DPP3	Dipeptidyl Peptidase 3
DPP3-MSN	DPP3-responsive mesoporous silica nanoparticles
FACS	Fluorescence Activated Cell Sorting
FITC-MSN	FITC-avidin-capped ADAM9-MSNs
FOLFIRINOX	fluorouracil, leucovorin, oxaliplatin, and irinotecan
HTRA1	HtrA Serine Peptidase 1
LDH	Lactate dehydrogenase
MSN	Mesoporous Silica Nanoparticles
PDI	Polydispersity index
PRSS23	Serine Protease 23
PTX	Paclitaxel
STAMBPL1	STAM Binding Protein Like 1

their inner core and outer surface can be modified to suit specific needs [6]. Notably, MSNs can be designed to incorporate *gatekeeper systems* that allow controlled release of the encapsulated drugs [7–9]. This design holds the potential to attenuate side effects by restricting drug release to the site of tumor cells.

Within the context of PDAC, several gatekeeper systems have been explored [5], of which protease activity-dependent configurations are especially interesting. The reason for this is the abundant stroma seen in PDAC, which is relatively rich in proteases [10–12]. Protease-responsive gatekeepers are designed using a peptide linker tailored to tumor-enriched proteases, tethered with biotin to the surface of MSNs, and are subsequently used to seal the MSN pores by the interaction between biotin and avidin after drug encapsulation. In theory, when reaching the tumor (stroma), protease activity catalyzes the cleavage of the peptide linker, leading to the release of the encapsulated drugs. We have previously identified a disintegrin and metalloprotease domain 9 (*ADAM9*) as a PDAC-enriched protease and reported the development of ADAM9-responsive MSNs (ADAM9-MSNs) [11,13]. Although the fact that these ADAM9-MSNs were highly effective against PDAC cells with limited side effects *in vitro*, no antitumor effect could be observed *in vivo* however [13].

In this paper we provide an explanation for the disappointing *in vivo* efficacy of ADAM9-MSNs by showing that ADAM9-MSNs are efficiently taken up by cells thereby making them inaccessible for extracellularly expressed ADAM9. We next aimed to exploit the efficient cellular uptake of MSNs by identifying PDAC-enriched intracellular proteases, and show that paclitaxel-loaded MSNs responsive to the intracellular protease CAPN2 efficiently killed PDAC cells with limited cytotoxicity towards non-tumor cells *in vitro*. Most importantly, opposed to ADAM9-MSNs, CAPN2-MSNs effectively limited tumor growth in preclinical murine PDAC models with limited toxicity.

2. Methods

2.1. Cell culture

Human PANC-1, BxPC-3, MIA PaCa-2, Capan-1, HPAF-II (all ATCC, Manassas, VA, USA), SH-SY5Y (kindly provided by Dr. J. van Nes, Amsterdam UMC, Amsterdam, The Netherlands), and murine KP2 cells (derived from pancreatic adenocarcinomas from p48-Cre/LSL-Kras^{G12D}/Tp53flox/flox mice, kindly provided by Dr. DeNardo, Washington University Medical School, St. Louis, MO, USA) were grown in DMEM (Lonza, Basel, Switzerland) supplemented with 10% fetal calf serum, 100 units/mL penicillin and 500 μg/mL streptomycin (all Lonza). SH-SY5Y culture medium was additionally supplemented with MEM non-essential amino acids (#11140050, ThermoFisher, Waltham, MA, USA). Cells were cultured in a humidified incubator at 37 °C and 5% CO_2. Monthly mycoplasma tests were performed on all cell lines.

2.2. Analysis of publicly available gene expression datasets

Datasets were derived from Gene Expression Omnibus (https://www.ncbi.nlm.nih.gov/gds) and analyzed using the R2 microarray analysis and visualization platform (http://r2.amc.nl). First, the 'Subcellular Localization' category of the Gene Ontology project on uniprot.org was assessed to differentiate all proteases into extracellular and intracellular proteases. Next, expression levels of intracellular proteases were derived from cell line datasets (GSE36133, GSE57083, and E-MTAB-783), PDAC datasets (GSE17891, GSE16515, GSE32676, GSE15471, GSE62452, and GSE36924; all containing both tumor and control pancreatic tissue), and datasets containing expression levels in lymphocytes (GSE46510), monocytes (GSE7158), leukocytes (GSE22886), macrophages (GSE2125), multiple hematopoietic subtypes (GSE24759), whole blood (GTeX v4), and healthy organs (GTeX v4). Average protease expression was calculated by averaging the expression level of every intracellular protease (n = 282) analyzed in all samples in a given dataset. Expression levels were considered to be high when they were above the average expression level plus 1.5 × the standard deviation of all proteases. To exclude effects from different gene expression analysis platforms and normalization methods comparative analyses were only performed within one dataset (except those using healthy organ datasets). Datasets using different gene expression (PDAC and healthy organs) analysis platforms were first normalized to b-actin expression before protease expression levels were compared.

2.3. Synthesis and surface modification of MSNs

MSNs were synthesized using the sol–gel emulsion essentially as described before [11]. In short, cetyltrimethylammonium bromide (CTAB, ≥99%, Sigma-Aldrich, Shanghai, China) and tetraethyl orthosilicate (TEOS, ≥99%, Sigma-Aldrich) were incubated for 2 h after which the surfactant CTAB was removed by overnight incubation in a methanol and hydrochloric acid. The resulting MSNs were filtered, washed, and dried under a high vacuum. Overnight refluxing by dried toluene (>99.3%, Honeywell Fluka, Seelze, Germany) and aminopropyl triethoxysilane (APTES, ≥99%, Sigma-Aldrich) resulted in surface amine grafting, followed by filtering and drying under vacuum to obtain MSN-NH$_2$. MSN-PEG$_4$-N$_3$ was obtained through overnight stirring of a suspension of MSN-NH$_2$ with N$_3$-PEG$_4$-COOH (1 eq., >97%, Biomatrik, Jiaxing, Zhejiang, China), HATU (2 eq., 99%, Alfa Aesar, Kendel, Germany), and DIPEA (3 eq., ≥99%, Sigma-Aldrich) in DMF (≥99.8%, Biosolve Chimie, Dieuze, France). After overnight incubation, the PEGylated MSNs were filtered, washed with water and ethanol, and subjected to transmission electron microscopy to confirm successful synthesis [11].

2.4. Synthesis, conjugation, and characterization of linker peptides

The synthesis and conjugation of linker peptides onto MSNs were similar as described before [11]. In summary, peptides (as shown in Table 2) were synthesized using a Liberty Blue automated, microwave-assisted, peptide synthesizer (CEM Corporation, Matthews, NC, USA). Except for Fmoc-propargyl-glycine (Glentham Life Sciences, Corsham, UK), Fmoc-homophenylalanine (Carbolution, St. Ingbert, Germany) and Fmoc-D-homophenylalanine (Alfa Aesar), all protected amino acids were acquired from Novabiochem (Darmstadt, Germany). All amino acids were Fmoc-deprotected by 20% piperidine (Biosolve Chimie) in DMF. Amide coupling to the deprotected amino acids was achieved by incubation of amino acids with diisopropylcarbodiimide (DIC, 99%, Acros Organics, Budapest, Hungary), and Oxyma Pure (Carl Roth, Karlsruhe, Germany). Finally, biotin was coupled to the peptide N terminus using biotin (≥99%, Sigma-Aldrich, lyophilized powder, St. Louis, MO, USA), HATU (99%, Alfa Aesar), and DIPEA (≥99%, Sigma-Aldrich). A mixture of trifluoroacetic acid (TFA, ≥99.5%, Biosolve Chimie), triisopropylsilane (TIPS, 98%, Sigma-Aldrich) and water was used to cleave the resin from the synthesized peptide linkers. The resulting peptide linkers were subsequently precipitated using cold diethyl ether (100%, VWR Chemicals BDH, Darmstadt, Germany) and purified using HPLC. After assessing the purity of the collected fractions by LC-MS the fractions were pooled and lyophilized. Finally, the linker peptides were conjugated to the MSNs by employing a copper-catalyzed click reaction. A suspension of anhydrous copper (II)sulfate (CuSO₄, ≥98%, ThermoFisher), sodium L-ascorbate (≥99%, Sigma-Aldrich), and tris(3-hydroxypropyltriazolylmethyl)amine (THPTA, Lumiprobe, Hunt Valley, MD, USA) in deionized water was flushed with nitrogen for 30 min, after which 10 μmol biotin-coupled linker peptides and 10 mg MSN-PEG₄-N₃ were added. The reaction mixture was then stirred overnight at room temperature in an inert atmosphere, after which the MSNs were centrifuged and washed with water and ethanol to obtain peptide-linker-functionalized MSNs.

Characterization of MSNs was performed as described in [11]. In short, dynamic light scattering (DLS) measurements were performed to assess the size of the MSNs, and Fourier transform infrared (FT-IR) spectroscopy and zeta potential (ZP) were used to confirm the successful synthesis and functionalization of the MSNs.

2.5. Cellular uptake of MSNs

For uptake experiments, 1 mg ADAM9-MSNs was incubated with Alexa Fluor 488-conjugated streptavidin for 30 min. Next, the MSNs were washed and stored at −70 °C until used for uptake experiments. For Fluorescence Activated Cell Sorting (FACS) experiments, 20.000 PANC-1, MIA PaCa-2 or BxPC-3 cells were seeded in a 96-well plate and left to attach overnight. The following day, the cells were incubated with various amounts of FITC-avidin-capped ADAM9-MSNs (FITC-MSN) for 30 min, 1 h or 2 h. Next, the medium was removed, cells were washed twice with PBS and incubated with 100 μL trypsin (Gibco, Thermo Fischer Scientific, Waltham, MA, USA). The detached cells were resuspended in 100 μL ice-cold PBS and analyzed for the presence of MSNs on a BD FACSCanto II (BD Biosciences, Franklin Lakes, NJ, USA). Data was analyzed using FLOWJO v10 (FlowJo LLC, Ashland, OR, USA). To

Table 1
Oligonucleotides used for quantitative PCR.

Oligonucleotide	Sequence
TBP forward primer	5′-atcccaagcggtttgctgc-3′
TBP reverse primer	5′-actgttcttcactcttggctc-3′
RPLPO forward primer	5′-ggcaccattgaaatcctgagtgatgtg-3′
RPLPO reverse primer	5′-ttgcggacaccctccaggaagc-3′
CDK4 forward primer	5′-tctatggtcgggcctctg-3′
CDK4 reverse primer	5′-tcagatcaagggagaccct-3′

Table 2
Overview of protease substrates.

Peptide	Sequence	Theoretical Mass (Da)	Measured m/z	Purity
ADAM9-biotin	Biotin-PRAAAF*TSPKGGG*	1493.74	1492.43	≥98%
BACE2-biotin	Biotin-SEVNLDAEFRGGG*	1613,71	1612,20	≥98%
CAPN2-biotin	Biotin-SGAGLPLFAARPGANSGGG*	1919,93	1919,05	≥99%
DPP3-biotin	Biotin-GGGDRVYIHPFGGG*	1651,76	1650,96	≥99%

F* = homophenylalanine; G* = propargylglycine.

confirm cellular uptake as assessed by FACS analysis confocal images were acquired by seeding 20.000 PANC-1, MIA PaCa-2 or BxPC-3 wells in a 8-chamber slide (Ibidi, Gräfelring, Germany) followed by 48 h attachment and incubation with 20 μL FITC-MSNs (1 mg/mL), after 1 h the cells were carefully washed twice and lysosomes were stained using LysoBrite Red (AAT Bioquest, Pleasanton, CA, USA) following manufacturers protocol and subsequently fixed with 4% paraformaldehyde in PBS. Next, the fixed cells were stained with DAPI (1 μg/mL) for 10 min and washed twice with PBS. Mounted slides were imaged using a SP8X confocal microscope (Leica Microsystems, Wetzlar, Germany) using Leica Application Suite (LAS) software.

2.6. Inhibition cellular uptake MSNs

To prevent cellular uptake by PEGylation, 1 mg of FITC-avidin-capped ADAM9-MSNs were incubated with 5, 10 or 30 mg PEG2000 (Sigma-Aldrich) coupled to biotin for 30 min. The PEG-biotin-conjugated FITC-MSNs were washed twice and resuspended in PBS. For uptake inhibition experiments 20.000 PANC-1 cells were seeded per well in a 96-well plate. After overnight attachment, the cells were incubated with 20 μL of control MSNs or 5, 10 or 30 mg PEG-biotin-conjugated FITC-MSNs for 30 min, 1 h or 72 h. After designated time points the cells were washed twice, detached using 100 μL trypsin and resuspended in 200 μL PBS and analyzed by FACS. Subsequently, PANC-1 cells were treated with various amounts of 30 mg PEG-biotin-conjugated FITC-MSNs for 1 h and analyzed using FACS as described above. As an alternative approach to PEGylation, cells were also pretreated for 20 min with 0.056 M sucrose (Sigma-Aldrich), 1 μM chloroquine (Sigma-Aldrich) or various concentrations of Dyngo-4a (Selleckchem, Houston, TX, USA). At various time points the pretreatments were removed and 20 μL FITC-MSNs in 100 μL added for 1 h. Cells were detached, resuspended and measured as described above. All data was analyzed using FLOWJO v10 (FlowJo LLC, USA).

2.7. Paclitaxel loading and capping of MSNs

Peptide-linker-functionalized MSNs were loaded with paclitaxel by the adsorption equilibrium method [14] and capped with avidin as described in [13]. In summary, paclitaxel (>99.5%, LC Laboratories, Woburn, ON, Canada) was dissolved at a concentration of 10 mg/mL, added to 1 mg of MSNs and incubated at 37 °C and 1200 rpm for 1.5 h. After 1.5 h the paclitaxel-loaded MSNs were centrifuged and capped by the addition of 1.5 mg avidin (EMD Millipore, Burlington, MA, USA) for 30 min. Finally, the capped MSNs were washed twice with water and ethanol and redispersed in HBSS (Gibco, ThermoFisher) at a concentration of 1 mg/mL. To increase the loading efficiency for *in vivo* experiments the various types of MSNs were loaded in 60 separate batches of 1 mg. Successful loading of paclitaxel was confirmed by incubating PANC-1 cells *in vitro* with multiple randomly selected loaded batches of ADAM9-MSNs, CAPN2-MSNs and DPP3-MSNs. As all loaded batches resulted in approximately 80% cell death (Supplemental Figs. 1 and 2), indicating the successful and uniform loading of paclitaxel, we pooled

the samples and assessed the cytotoxicity *in vivo*. Loaded MSNs were centrifuged to measure the UV absorbance of the supernatant to determine the amount of unloaded paclitaxel. The supernatant was dried and resolved in 1.75 mL dimethylsulfoxide (DMSO, Sigma-Aldrich, Steinheim, Germany) and UV absorbance was measured at 263 nm using a Cary 300 UV–Vis spectrometer (Agilent Technologies, Santa Clara, CA, USA).

2.8. PDAC cytotoxicity assays

3500 PANC-1, 7500 Capan-2, or 3000 KP2 cells were seeded in single wells of a 96-well plate and left to attach overnight. Next, the cells were incubated with different concentrations of free paclitaxel, capped paclitaxel-loaded BACE2-MSNs, CAPN2-MSNs or DPP3-MSNs. To test MSN stability and integrity, MSNs were incubated for various durations while shaking at 800 rpm at 37 °C prior to administration. Additionally, paclitaxel-loaded MSNs were stored for up to two years at −20 °C prior to cell treatment. After three days, the cells were washed, incubated with crystal violet (0.5% crystal violet, 3% formaldehyde in dH_2O) for 20 min at room temperature, followed by aspiration of the crystal violet solution, washing three times with tap water and solubilization of the formed crystals by addition of 100 μL DMSO (Merck). After 20 min of incubation on a plate shaker at room temperature, the absorbance was measured at 600 nm on a Synergy HT plate reader (Biotek Instruments, Winooski, VT, USA).

2.9. Neurotoxicity assay

SH-SY5Y (1000) cells were seeded in single wells of a 96-well plate and left to attach for 48 h. To induce differentiation into a neuronal phenotype the cells were incubated with 1 μM all-trans retinoic acid (ATRA; #R2625-50 MG, Merck, Rahway, NJ, USA) for 48 h. After 48 h, various concentrations of free paclitaxel, capped paclitaxel-loaded CAPN2-MSNs, or DPP3-MSNs were administered. After three days, the cells were incubated with 20 μL CellTiter-Blue (Promega, Leiden, The Netherlands) for 3 h and fluorescence was measured at 590 nm on a Synergy HT plate reader.

2.10. Bone marrow cell toxicity

To test the toxicity of free paclitaxel and paclitaxel-loaded MSNs on bone marrow cells a similar approach as described before [13] was employed. To recap, freshly excised C57BL/6 (Charles River Laboratories, Wilmington, MA, USA) murine hind limbs were washed in 70% ethanol, transferred to a Petri dish containing ice-cold sterile PBS and subsequently collected in a 50 mL Falcon tube by cutting the femur and tibia at both ends with sterile scissors and flushing the bones with ice-cold sterile PBS. After dispersing the bone marrow, the red blood cells were lysed using erythrocyte lysis buffer (buffer EL; #79217, Qiagen, Venlo, The Netherlands) and the remaining bone marrow cells were resuspended in ice-cold sterile PBS and counted. Finally, a total of 90,000 cells were added to 3 mL mouse methylcellulose complete medium (#HSC007, R&D Systems, Minneapolis, MN, USA) containing multiple concentrations of free paclitaxel, CAPN2-MSNs, or DPP3-MSNs before plating 1 mL medium/well in a 12-well plate. After a week of incubation at 37 °C, the number of colonies was counted.

2.11. Animals

Female C57BL/6 (Charles River Laboratories, Wilmington, MA, USA) and female NOD-scid IL2rγnull mice (NSG mice, bred at our facility) were housed at the Amsterdam University Medical Center's (AUMC) animal facility. All animals had access to water and food ad libitum. All animal experiments were approved by the Institutional Animal Care and Use Committee of the AUMC according to protocol DIX-19-9064.

2.12. Antitumor efficacy of paclitaxel-loaded MSNs

Either 25.000 KP2 or 2×10^6 PANC-1 cells in a 1:1 mixture of DMEM and Matrigel were subcutaneously injected in the left flank of C57BL/6 mice or NSG mice, respectively. One week after tumor cell injection, the mice were randomly assigned to receive PBS, 20 mg/kg free paclitaxel, 30 mg/kg free nab-paclitaxel, or 50 mg/kg paclitaxel-loaded ADAM9-MSNs, CAPN2-MSN or DPP3-MSN by intravenous injection in a total volume of 100 μL. All KP2 mice were treated twice weekly for 4 weeks, with a total of 7 injections. All PANC-1 mice received a total of 5 injections over the course of 2.5 weeks. Changes in body weight and tumor growth were tracked using a scale and caliper three times a week. Two days after receiving the last injection the mice were killed or upon reaching humane endpoints specified as tumor size >1.5 cm³, ulceration, acute weight loss >15% within two days, chronic weight loss of >15% combined with visual discomfort, or chronic weight loss of >20% without any signs of discomfort. Blood collected by heart puncture was centrifuged at 3500 rpm for 10 min at 4 °C, and plasma was collected and stored at −70 °C. Tumors were excised and divided in two, half was immediately frozen using liquid nitrogen and stored at −70 °C, the other half was fixed using 4% formaldehyde (Klinipath, Duiven, The Netherlands) before paraffin-embedding.

2.13. Quantitative PCR

Tumors were homogenized in 300 μL lysis buffer (Nucelospin TriPep kit; Macherey-Nagel, Duren, Germany) using Tissuelyser LT (Qiagen) at 50 Hz for 2 min. RNA was isolated using the NucleoSpin TriPep kit according to the manufacturer's protocol (Macherey-Nagel). Eluted RNA was analyzed spectrophotometrically using the Nanodrop 2000. Next, RNA samples were treated with RQ1 RNAse-free DNAse (Promega Benelux BV, Leiden, the Netherlands) and reverse transcribed into cDNA using M-MLV reverse transcriptase (Promega Benelux BV), random hexamers (Promega Benelux BV) and 10 mM dNTP Mix (Thermo Scientific, Waltham, MA). Quantitative real-time PCR (qPCR) was performed using Sensifast SYBR No-ROX kit (GC Biotech, Waddinxveen, The Netherlands) on a Lightcycler 480 II (Roche Molecular systems, Inc., Almere, the Netherlands) according to manufacturer's instructions. *CDK4* expression levels were normalized to the expression of the reference genes TBP and RPLPO using the primers listed in Table 1.

2.14. Immunohistochemistry

Formalin-fixed paraffin-embedded tumors were sectioned to 5 μM slices on a Leica RM2245 microtome (Leica Biosystems, Nussloch, Germany). Tissue sections were deparaffinized and antigen retrieval was performed using 10 mM sodium citrate solution pH (MedChemExpress, Monmouth Junction, NJ, USA). Next, slides were stained for H&E or incubated with 3% hydrogen peroxide in PBS to block endogenous peroxidase activity for cleaved caspase-3 staining. The primary antibody anti-cleaved caspase-3 (#9961, Cell Signaling, Danvers, MS, USA) was diluted 1:500 in BrightDiluent (Immunologic, Arnhem, The Netherlands), applied on tissue sections and incubated overnight at 4 °C in a humidified chamber. The next day, slides were washed with PBS and amplification of signal was achieved by addition of BrightVision post antibody block (DPVR-55HRP, Immunologic). After 30 min the post antibody block was washed away with PBS and secondary antibody Bright-DAB (BS04-999, Immunologic) was added for 3 min at room temperature. Finally, slides were washed for 2 min with PBS, counterstained with 100% haematoxylin (Klinipath) for 2 min, rinsed with dH2O for 2 min, dehydrated using ethanol and xylene, and finally mounted with Pertex (Klinipath). Stained slides were imaged on a IntelliSite Ultra Fast 1.6 slide scanner (Philips, Eindhoven, The Netherlands). Quantification of cleaved caspase-3 was performed using QuPath (version 0.5.0) [15]. The 'positive cell detection' analysis tool was used modifying the following parameters: **Setup parameters:**

Detection image – Optical density sum; **Nucleus parameters:** *Background radius* – 5 μm; **Intensity parameters:** *Threshold* – 0.05; **Intensity threshold parameters:** *Score compartment* – Cell DAB OD max.

2.15. Biochemical analysis

Plasma glucose, creatinine, urea, aspartate aminotransferase (ASAT), alanine aminotransferase (ALAT), and lactate dehydrogenase (LDH) levels were measured at the clinical diagnostics laboratory of the AUMC.

2.16. Peptide cleavage assay

Dabcyl- and FAM-modified linker peptides containing ADAM9 (PRAAAF*TSPK), BACE2 (SEVNLDAEFR), CAPN2 (SGAGLPLFAARP-GANS) or DPP3 (DRVYIHPF) cleavage sites were purchased from GL Biochem (Shanghai, China). 1 μM peptide was incubated with 100 μL PBS or PANC-1 cell lysate (1×10^6 cells/mL). Fluorescence was measured every 15 min at Ex/Em 484/530 nm wavelengths using a Biotek Synergy HT plate reader (Biotek Instruments, Winooski, VT, USA).

2.17. Statistical analyses

Statistical analyses were performed using GraphPad Prism 6.0 (GraphPad Software Inc., La Jolla, CA, USA). For *in vitro* experiments, two-tailed *p*-values were calculated by unpaired *t*-test and One-way ANOVA. Two-way ANOVA was used to compare tumor growth curves. Significance was set at p < 0.05.

3. Results

3.1. ADAM9-MSNs are efficiently internalized by PDAC cells

We have previously reported the development of optimized ADAM9-responsive MSNs (here referred to as ADAM9-MSNs) specifically targeting PDAC cells [13]. Although these ADAM9-MSNs very efficiently induced PDAC cell death with limited bone marrow- and neurotoxicity *in vitro*, anti-tumor efficacy *in vivo* was lacking. Considering that ADAM9 tends to be localized in the extracellular matrix [16], we hypothesized that internalization of ADAM9-MSNs might be responsible for the observed lack of tumor response *in vivo*. To test this hypothesis, we capped empty ADAM9-MSNs with Alexa Fluor 488-conjugated avidin (FITC-MSNs) and incubated PANC-1, MIA PaCa-2 and BxPC-3 PDAC cells with various amounts for several periods of time. After removing the MSNs, the presence of FITC-MSNs in the cells was assessed using Flow Cytometry. In these experiments, we observed a dose-dependent increase in the proportion of FITC-positive cells over time (Fig. 1A and B). To validate that FITC positivity was indeed due to cellular uptake, confocal microscopy was employed which revealed the internalization of FITC-MSNs across all tested cell lines (Fig. 1C). Treatment of PANC-1 cells with fluorescein-*loaded* MSNs capped with normal avidin also resulted in efficient cellular uptake, indicating that the FITC-moiety on the periphery of FITC-MSNs did not influence uptake mechanisms (Supplemental Fig. 3). It is thus very likely that the cellular uptake of ADAM9-MSNs might have hampered anti-tumor efficacy *in vivo* by limiting the exposure of these MSNs to the extracellular ADAM9 with consequent limited drug release. In an effort to improve the exposure of ADAM9-MSNs to ADAM9, we explored strategies to impede the internalization of our MSNs. Unfortunately, the introduction of PEG-2000 to the MSN, aimed to increase systemic circulation time, did not decrease the internalization of the MSNs (Supplemental Fig. 4). In addition, the
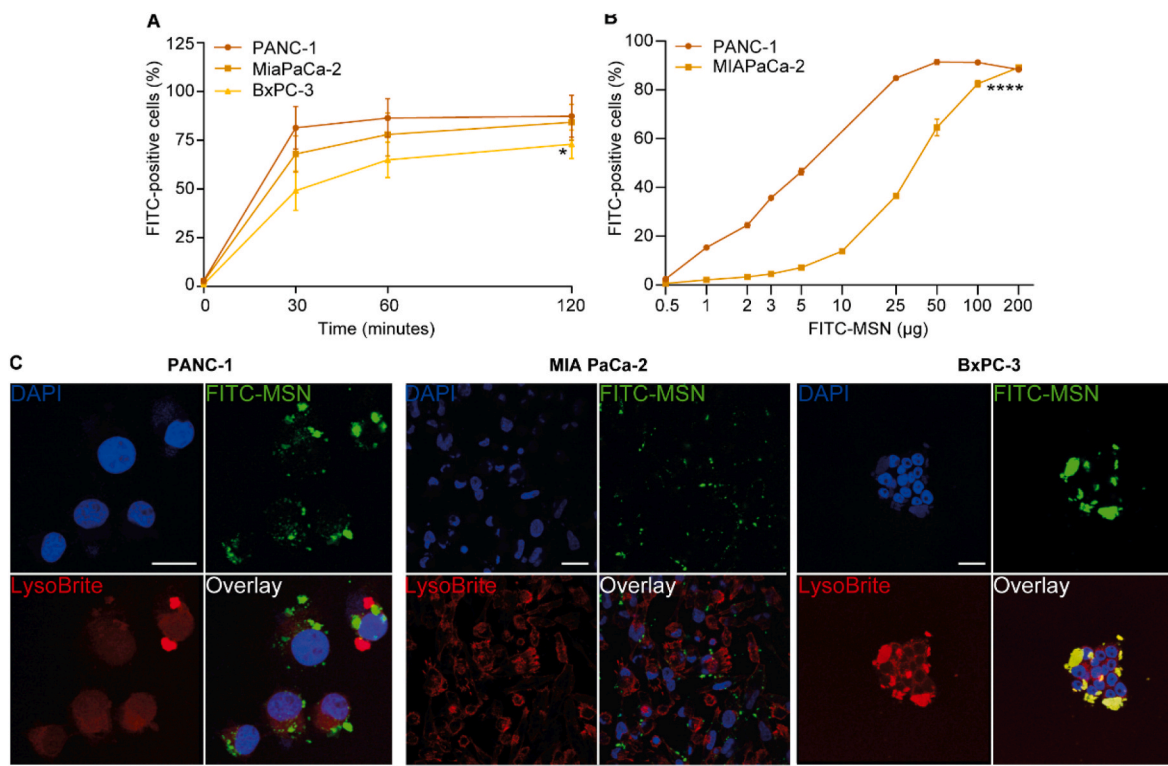
Fig. 1. FITC-avidin-capped ADAM9-MSNs are efficiently taken up by PDAC cells. Cellular uptake of FITC-MSNs by PDAC cells after various incubation periods (**A**) and concentrations (**B**). Data are shown as the mean of three representative experiments with $n = 3$. Results are normalized to untreated controls. Scale bars = 25 μM. Two-way ANOVA was used to compare MSN uptake. Levels of significance: *p < 0.05, ****p > 0.0001. (**C**) Confocal Images showing cellular uptake of FITC-MSNs. Blue; DAPI, Red; LysoBrite (lysosomal staining), Green; FITC-MSN.

pre-treatment of cells with well-known compounds that target cellular uptake mechanisms like dyngo-4a, sucrose and chloroquine did also not reduce cellular uptake (Supplemental Figs. 5A–C).

3.2. Identification of PDAC-enriched intracellular proteases

As we were unable to inhibit the cellular uptake of ADAM9-MSNs, we envisioned that modifying the MSNs with a peptide linker responsive to *intracellular* proteases could increase the cytotoxic potential. To this end, we first queried the subcellular localization of all 571 proteases expressed by the human genome [17], resulting in the identification of 282 *intracellularly* expressed proteases (Fig. 2A). Subsequent analysis aimed to identify proteases that were overexpressed in at least two out of three comprehensive PDAC cell line datasets, hereto we examined the expression patterns among the aforementioned 282 proteases in three datasets, encompassing a combined total of 101 samples derived from 51 distinct PDAC cell lines, and identified a total of 156 proteases that were overexpressed (Fig. 2B). To streamline the number of candidates we proceeded to evaluate the gene expression levels in PDAC tissues obtained from patients. Of the 156 proteases assessed in the cohort, 141 exhibited increased expression levels compared to the average expression of all proteases in PDAC in five out of six databases. Importantly, 15 candidates showed an average 1.5-fold higher expression in PDAC relative to adjacent non-tumor tissue (Fig. 2C). A literature search into all the remaining candidates led us to exclude Abhydrolase Domain Containing 17C, Depalmitoylase (*ABHD17C*) from further analysis, as ABHD17C is a palmitoylase involved in post-translational attachment of palmitate to cysteine residues and therefore not involved in cleaving peptide substrates [18]. To obtain PDAC-specificity we analyzed the expression levels of the 14 remaining candidate proteases in multiple hematopoietic subsets, resulting in the exclusion of 8 proteases that were found to be expressed in multiple cellular constituents of the blood compartment (Fig. 2D). Finally, the expression levels of the remaining 6 intracellular proteases were assessed in healthy tissue. Five of the six candidates generally showed limited expression in healthy organs and only one protease, HtrA Serine Peptidase 1 (*HTRA1*), was expressed abundantly across several organs (Fig. 2E–J), resulting in its exclusion. This selection process yielded five potential candidates, namely Beta-Secretase 2 (*BACE2*), Calpain 2 (*CAPN2*), Dipeptidyl Peptidase 3 (*DPP3*), Serine Protease 23 (*PRSS23*) and STAM Binding Protein Like 1 (*STAMBPL1*). For three of the 5 identified PDAC-enriched intracellular proteases, protease substrates have been described in literature (i.e. BACE2 [19], CAPN2 [20] and DPP3 [21]; Table 2) based upon which we decided to synthesize BACE2-, CAPN2- and DPP3-responsive MSNs. Successful synthesis was confirmed by dynamic light scattering, zeta potential measurements, and Fourier-transform infrared spectroscopy (Table 3, Supplemental Fig. 6). Functionalization with the biotin-conjugated CAPN2- and DPP3-peptide linker resulted in an increase of ZP to 25.47 +- 0.76 mV, and 22.9 +- 1.65 mV, respectively, whereas biotin-conjugated BACE2-peptide linker led to a decrease of ZP to −26.9 +- 0.24, caused by the majority of anionic amino acids in this peptide. As expected, the particle size does not change significantly after the functionalization (Table 3).

3.3. Paclitaxel-loaded CAPN2- and DPP3-MSNs show high anti-cancer efficacy while reducing potential side effects in vitro
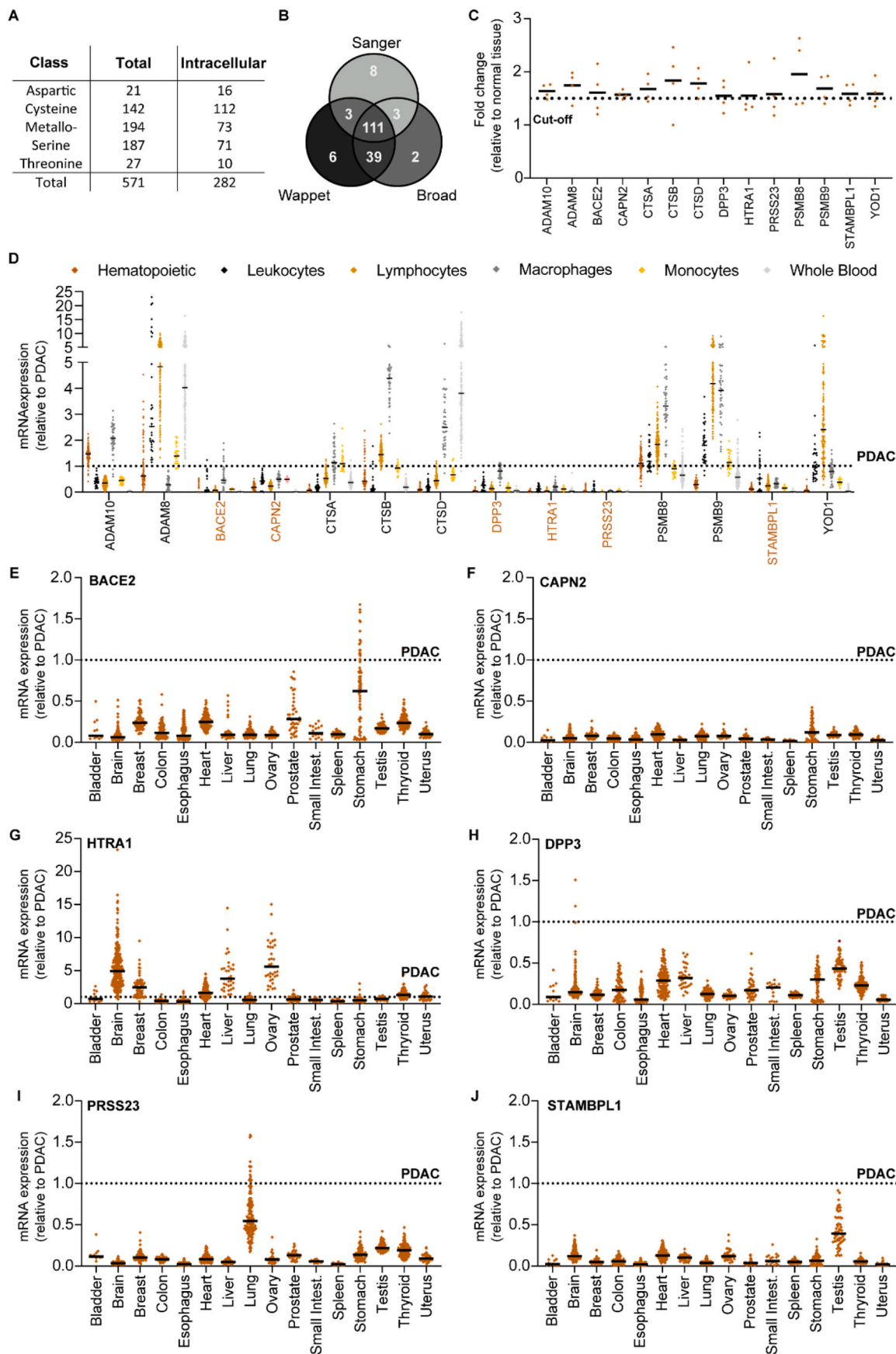
Essential to the successful generation of protease-responsive MSNs is the release of loaded chemotherapeutics by PDAC cells. To test this, we loaded the MSNs with paclitaxel (Supplemental Table 1), a first-line treatment against PDAC, and treated PANC-1, Capan-1 and HPAF-II cells with increasing amounts of MSNs. As expected, CAPN2- and DPP3-responsive MSNs induced cell death in a dose-dependent manner in all cell lines tested (Fig. 3A–C, 3E-G). Of note, even at 16-fold higher concentrations, BACE2-MSNs failed to induce significant cell death in HPAF-II or PANC-1, indicating that neither cell line is capable of

efficiently cleaving the peptide linker and releasing the loaded paclitaxel (Fig. 3I and J). Critical to the success of targeted therapy is the stability of MSNs. We employed Transmission Electron Microscopy two years after synthesis/−70C storage and confirmed morphological stability of CAPN2- and DPP3-MSNs (Supplemental Figs. 7A and D). Subsequent treatment of PANC-1 cells with similar amounts of CAPN2- and DPP3-MSNs two years after the original experiments show similar dose-dependent cell killing (Supplemental Figs. 7B and E), indicating biochemical integrity of the gatekeeper system. To assess MSN stability at physiological temperatures and to mimic conditions of *in vivo* experiments, MSNs were incubated at 37 °C for up to 48 h before administration to PANC-1 cells. Of note, MSN-induced cell death was similar in all conditions, implying stability at body temperature for at least two days (Supplemental Figs. 7C and F).

Neurotoxicity and leukopenia are two common side effects of paclitaxel. Given that the overarching objective of targeted drug delivery is to mitigate such side effects, we proceeded to evaluate the toxicity of the generated MSNs towards neuronal cells and leukocytes. First, we treated the neuronal cell line SH-SY5Y with amounts of MSNs that robustly induced cell death in PDAC cell lines. Encouragingly, even at the highest doses administered no cell death of SH-SY5Y cells was observed when treated with DPP3-MSNs (Fig. 3H). While some degree of toxicity was apparent from CAPN2-MSNs (Fig. 3D), this was much lower than the effects on PANC-1 and Capan-1 cells (Fig. 3B and C). Of note, previous results found that SH-SY5Y cells were more sensitive to paclitaxel than PDAC cells, further strengthening the observed results [5]. No difference in toxicity could be observed between SH-SY5Y and PANC-1 or HPAF-II cell lines when treated with BACE2-MSNs (Fig. 3I–K). The lack of specificity and efficacy of BACE2-MSNs led us to pursue it no further. As the results of CAPN2- and DPP3-MSNs were promising outcomes, we next assessed their impact on bone marrow-derived leukocytes (BMDL) at concentrations that induced 80% cell death in PANC-1 cells. No reduction in colony count was evident following 7 days of treatment with either CAPN2- or DPP3-MSNs (Fig. 3L). In stark contrast, 20 nM of free paclitaxel led to nearly a 40% reduction in colony numbers. In summary, CAPN2- and DPP3-MSNs induce efficient PDAC cytotoxicity while simultaneously reducing neurotoxicity and leukopenia *in vitro*.

3.4. CAPN2-MSNs show promising anti-tumor efficacy without adverse effects in vivo

Since both CAPN2- and DPP3-responsive MSNs showed *in vitro* efficacy and specificity we next tested their applicability *in vivo*. As we have previously confirmed the delivery of MSNs to subcutaneous tumors and determined the optimal dosage and treatment schedule [13], we decided to use a similar experimental design. Prior to the *in vivo* experiment, we ensured that the injected KP2 cells were capable of opening and releasing the paclitaxel from the CAPN2- and DPP3-MSNs *in vitro*. Indeed, this was found to be the case, albeit less extensive than in PANC-1 and Capan-1 cells (Fig. 4A and B). Similar to [13], the evaluation of *in vivo* antitumor efficacy and mitigation of side effects involved subjecting mice to a regimen of seven intravenous administrations in the tail with paclitaxel-loaded CAPN2- or DPP3-MSNs (50 mg/kg), distributed over three weeks. Control mice were treated with either PBS or free paclitaxel at a dose of 20 mg/kg, as established in [32]. All mice were treated exactly one week after subcutaneous tumor grafting. Throughout the experiment, body weight and tumor volumes were monitored. Notably, among the mice treated with free paclitaxel, a considerable majority of two out of three exhibited severe adverse effects, leading to discernible weight reduction (Fig. 4C), necessitating their removal from the experiment. The antitumor efficacy of CAPN2-MSN and free PTX were found to be comparable, while DPP3-MSN-treated mice displayed no reduction in tumor volume (Fig. 4D). Notably, administration of free PTX delayed tumor growth, but in time tumor growth recommenced. This phenomenon mirrors the frequently observed initial positive

A

Class	Total	Intracellular
Aspartic	21	16
Cysteine	142	112
Metallo-	194	73
Serine	187	71
Threonine	27	10
Total	571	282

(caption on next page)

Fig. 2. Identification of PDAC-enriched *intracellular* proteases through bioinformatics analysis. (**A**) Overview of all proteases in the human genome and the number of intracellular proteases included in the analysis. (**B**) Venn diagram illustrating proteases with above-average expression in all PDAC cell lines from Sanger (E-MTAB-783 [22]), Wappet (GSE57083), and Broad (GSE36133 [23]) datasets. (**C**) Fold-change in expression levels of candidate proteases in patient-derived tumor biopsies compared to healthy adjacent pancreas sections from four datasets (GSE15471 [24], GSE62452 [25], GSE16515 [26] and GSE32676 [27]). The cutoff is set at a 1.5-fold increase, indicated as a dotted line. (**D**) Expression levels of selected candidate proteases in healthy blood components relative to their expression levels in PDAC, including hematopoietic subtypes (GSE24759 [28]), leukocytes (GSE22886 [29]), lymphocytes (GSE46510 [30]), macrophages (GSE2125 [31]), monocytes (GSE7158), and whole blood (GTEx v4) datasets. (**E-J**) Expression levels of remaining candidate proteases in healthy organs (GTEx v4) relative to their expression level in PDAC, represented by a dotted line set at 1.

Table 3
Characterization of generated MSNs. Hydrodynamic size, polydispersity index (PDI), and zeta potential of MSNs, MSN-NH$_2$, MSN-PEG$_4$-N$_3$, and peptide linker functionalized MSNs in water measured by dynamic light scattering.

Sample	Size ± st.dev. (d.nm)	PDI	ZP ± st.dev. (mV)
MSNs	223.6 ± 62.1	0.36	−18.9 ± 0.1 [13]
MSN-NH2	191.5 ± 42.2	0.69	19.1 ± 0.7 [13]
MSN-PEG4-N3	233 ± 59.4	0.38	0.6 ± 4.3 [13]
ADAM9-MSN	210.6 ± 60.8	0.14	30.5 ± 1.2 [13]
BACE2-MSN	240.6 ± 72.4	0.35	−26.9 ± 0.2
CAPN2-MSN	235.1 ± 79.2	0.29	25.5 ± 0.8
DPP3-MSN	285.2 ± 99.7	0.47	22.9 ± 1.7

responses in patients, followed by therapy-resistant tumor growth.

In blood samples collected during the experiment, we were able to address whether the targeted delivery of paclitaxel through CAPN2- and DPP3-MSNs reduced levels of circulating markers for toxicity compared to free PTX. Compared to the control treatment, a decrease in leukocyte viability was observed, however compared to free PTX both CAPN2- and DPP3-MSNs treatment resulted in less leukopenia (Fig. 4E). Additionally, blood plasma levels of lactate dehydrogenase (LDH), and alanine aminotransferase (ALAT) were markedly increased in free PTX-treated mice, indicating that general organ damage was prevented by encapsulation of PTX (Fig. 4F and G). Plasma creatinine levels remained consistent in all treatment groups, indicating that no kidney damage was induced by either free PTX or MSNs (Fig. 4H). These results show that CAPN2-MSNs exhibit similar antitumor efficacy as free PTX but with much less toxicity. DPP3-MSNs showed similar patterns of reduced side effects, however, no antitumor effect could be observed.

It is crucial to highlight that among the total of 26 mice enrolled, 16 reached predefined humane endpoints (including ulceration and tumor sizes exceeding 1.5 cm^3) and had to be taken out of the experiment. The necessity of culling these animals impacted the analysis. To validate the promising efficacy of CAPN2-MSNs, an additional *in vivo* experiment
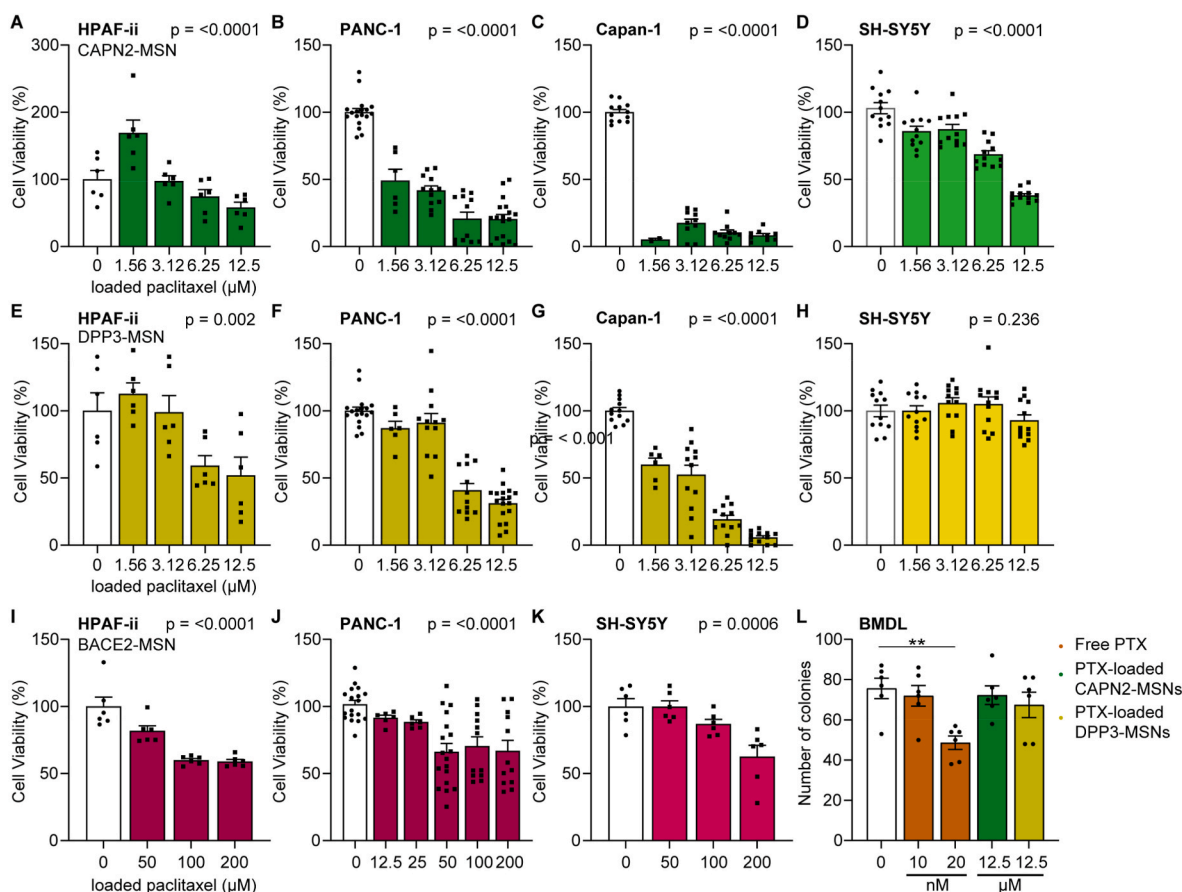
Fig. 3. CAPN2- and DPP3-responsive MSNs efficiently kill PDAC cells and reduce side effects *in vitro*. Cytotoxicity of paclitaxel-loaded CAPN2-MSNs in HPAF ii ((**A**), n = 6), PANC-1 ((**B**), n = 12), Capan-2 ((**C**), n = 12) and SH-SY5Y cells ((**D**), n = 12) after 72 h. Cytotoxicity of paclitaxel-loaded DPP3-MSNs in HPAF ii ((**E**), n = 6), PANC-1 ((**F**), n = 12), Capan-2 ((**G**), n = 12) and SH-SY5Y cells ((**H**), n = 12) after 72 h. Cytotoxicity of paclitaxel-loaded BACE2-MSNs in HPAF ii ((**I**), n = 6), PANC-1 ((**J**), n = 12) and SH-SY5Y cells ((**K**), n = 6) after 72 h. (**L**) Cytotoxicity of paclitaxel-loaded CAPN2- and DPP3-MSNs in bone marrow cells (n = 6) after 7 days. Data are normalized to untreated controls. Significance was determined by One-way ANOVA. Levels of significance: ns = not significant, **p < 0.01. BMDL: Bone Marrow-Derived Leukocytes.
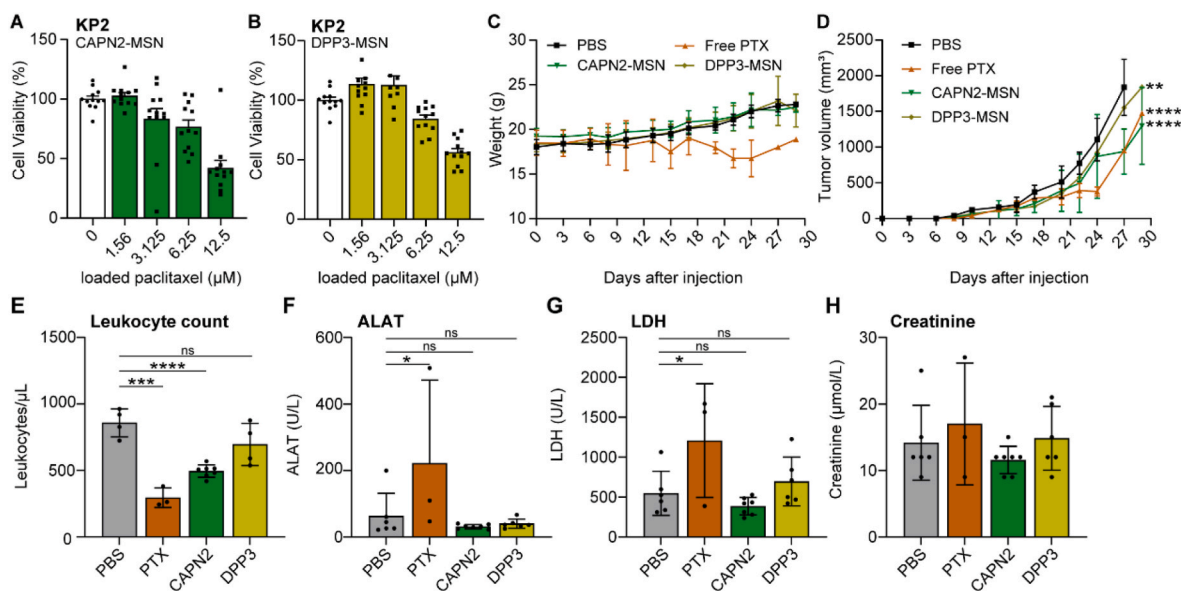
Fig. 4. Paclitaxel-loaded CAPN2-MSNs inhibit tumor growth and reduce neutropenia and organ damage in KP-2 tumor-bearing mice. *In vitro* cytotoxicity of paclitaxel-loaded CAPN2-MSNs (**A**) and DPP3-MSNs (**B**) on KP-2 cells 72 h after administration ($n = 12$). (**C**) Weight of mice plotted over time. (**D**) Tumor volume (mm^3) during the experiment. (**E**) Blood leukocyte counts at culling. Plasma ALAT (**F**), LDH (**G**) and creatinine (**H**) levels in mice treated with for PBS ($n = 6$), nab-PTX ($n = 3$), CAPN2-MSN ($n = 7$) and DPP3-MSN ($n = 6$) as measured by HPLC following standardized clinical guidelines of the AUMC. Two-tailed *p*-values for leukocyte counts, plasma ALAT and LDH were calculated by unpaired *t*-test. Two-way ANOVA was used to compare tumor growth curves. Levels of significance: ns = not significant, *$p < 0.05$, **$p < 0.01$, ****$p > 0.0001$. Data representing PBS- and free PTX groups have been reused from a previous publication [13]. Data analysis is similarly complicated as described in the legend of Fig. 4.

was planned using human PANC-1 cells instead of murine KP2 cells. Hereto, 2x10^6 PANC-1 cells were injected into the left flank of immune-deficient NSG mice. One week after tumor cell grafting a total of six injections were administered over the course of 2.5 weeks. Although ADAM9-and DPP3-MSNs demonstrated negligible antitumor efficacy we opted to include both MSNs as negative controls (at a dosage of 50 mg/kg). Additionally, we changed from unmodified free PTX to nab-paclitaxel (at 25 mg/kg) to mimic the human clinical setting more accurately. No treatment affected general well-being, as reflected in the absence of weight loss during the experiment, a trend consistent across other treatment groups (Fig. 5A). At the end of the experiment, a remarkable 68% reduction in tumor volume was observed in the CAPN2-MSN group compared to the PBS-treated group, which was twice the effect of the free nab-PTX-treated mice (33%; Fig. 5B). The decrease in tumor volume caused by free nab-PTX and CAPN2-MSNs becomes more pronounced when individual mice are considered (Fig. 5C–G). As anticipated, and confirming previous outcomes, neither ADAM9-or DPP3-MSNs showed substantial antitumor efficacy nor toxicity. In line with reduced tumor growth, cyclin-dependent kinase 4 (CDK4) mRNA levels were significantly reduced in CAPN2-MSN-treated mice compared to PBS and PTX treated mice (Fig. 5H). In addition, levels of cleaved caspase-3, a commonly used apoptotic marker, were increased in tumors of CAPN2-MSN-treated mice as compared to tumors of PBS treated mice (Fig. 5I). Quantification of the percentage cleaved caspase-3-positive cells showed a significant increase in CAPN2-MSN-treated tumors compared to control PBS (Fig. 5J). Together, the reduced cell proliferation and increased apoptosis observed after CAPN2-MSNs treatment most likely explains the decreased tumor size.

Analysis of plasma markers for pancreatic (glucose), kidney (urea and creatinine), liver (alanine aminotransferase; ALAT and aspartate aminotransferase; ASAT) and general organ (lactate dehydrogenase; LDH) damage revealed no off-target toxicity, corroborating the results from the KP2 *in vivo* experiment (Fig. 6A–F). In line, no histopathological signs of organ damage were evident on H&E stained pancreatic and colon sections (Fig. 6G). Collectively, these results underscore the benefit of systemic MSN administration, and more importantly, validate

the promising potential of CAPN2-MSNs in terms of both antitumor efficacy and the reduction of paclitaxel-induced side effects.

4. Discussion

The effectiveness of existing therapies in patients diagnosed with PDAC is hampered by unfavorable cytotoxicity profiles. The selective targeting of tumor cells without affecting healthy cells holds potential to decrease instances of treatment discontinuation and dose adjustments, thereby resulting in enhanced treatment efficacy. This would diminish PDAC-related mortality and morbidity, and the associated healthcare expenses. We have previously reported a novel MSN susceptible to the proteolytic activity of ADAM9 [11], however, despite optimization of the ADAM9-MSN *in vivo* administration did not result in antitumor efficacy [13]. In this paper, we show that the cellular uptake of ADAM9-MSNs is efficient, leading us to propose that their efficacy might be hampered by the inability of the particles to remain in the vicinity of the extracellularly deposited ADAM9. Next, we wondered if taking advantage of the cellular uptake and the design of MSNs responsive to *intracellular* proteases would improve the anti-tumor potential. We identified three promising candidate proteases, BACE2, CAPN2 and DPP3, of which peptide substrates were reported in literature. Subsequent assessment of anti-tumor efficacy and side effects *in vitro* and *in vivo* identified CAPN2-responsive MSNs as a promising candidate for the treatment of PDAC.

Here, we addressed challenges in the antitumor effectiveness of ADAM9-MSNs, considering the potential impediments posed by PDAC's desmoplastic reaction. We tested the hypothesis that cellular uptake might deplete MSNs from the tumor's extracellular matrix and hinder their interaction with ADAM9, finding that within 30 min, a majority of cells exhibited efficient MSN cellular uptake, confirmed through FACS and confocal images. It is however important to note that *in vitro* experiments happen under static conditions, increasing the exposure time of the MSNs to the cells as compared to *in vivo* experiments involving a blood flow and complex 3D architecture. It is therefore imaginable that the *in vitro* uptake is an overestimation, however, it is obvious that the
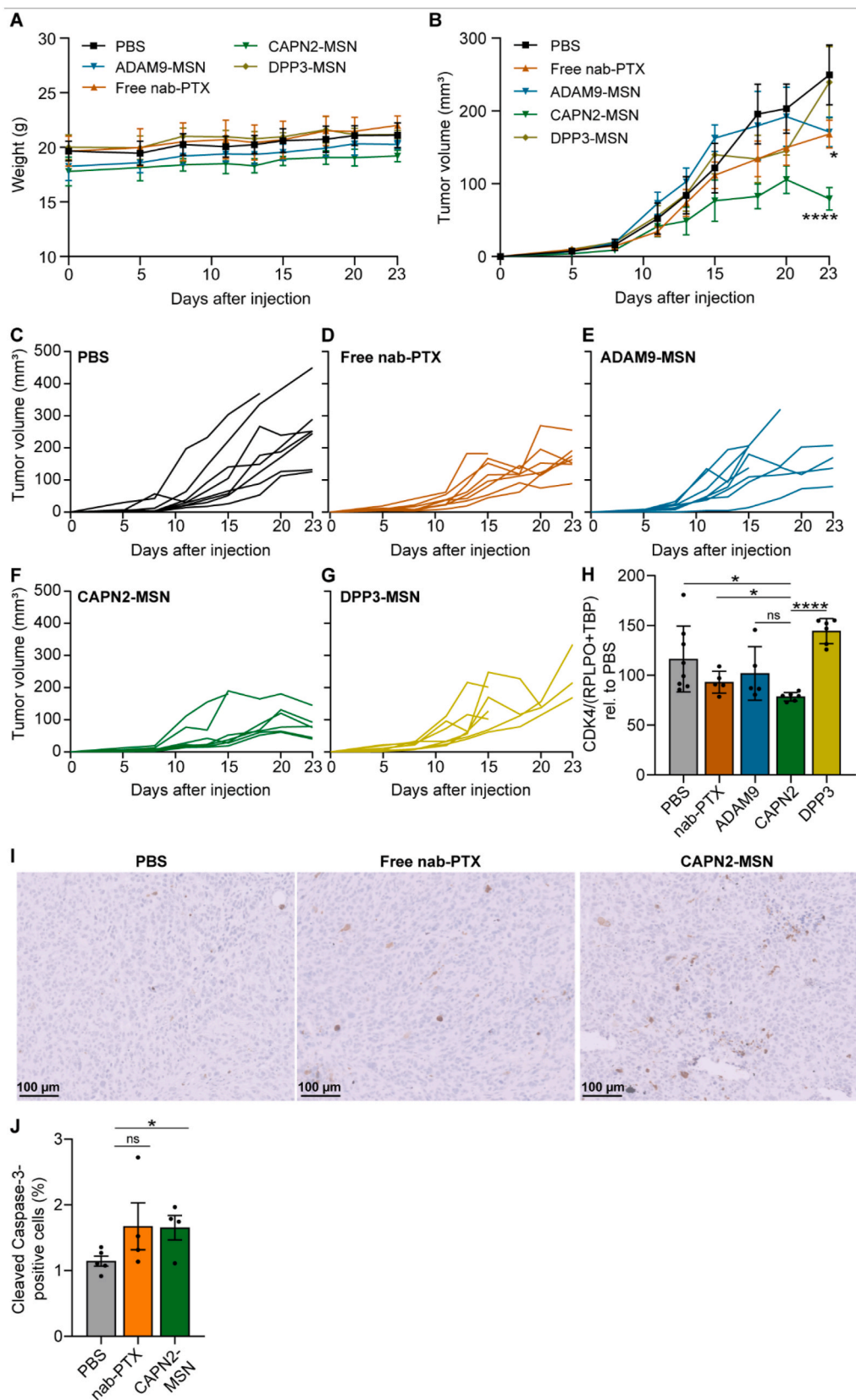
Fig. 5. Paclitaxel-loaded CAPN2-MSNs greatly reduce human PDAC cell growth *in vivo*. (**A**) Weight of mice during the experiment. (**B**) Tumor volume (mm^3) plotted over time. Tumor growth of individual mice treated with (**C**) PBS, (**D**) free nab-paclitaxel, (**E**) ADAM9-MSNs, (**F**) CAPN2-MSNs or (**G**) DPP3-MSNs. (**H**) CDK4 expression levels normalized to housekeeping genes TBP and RPLPO in tumors from PBS ($n = 7$), nab-PTX ($n = 5$), ADAM9-MSN ($n = 5$), CAPN2-MSN ($n = 6$) and DPP3-MSN ($n = 6$) treated mice. (**I**) Representative images of cleaved capase-3 stained tissue sections. Scale bar = 100 μM. (**J**) Quantification of cleaved caspase-3 positive cells in tumors treated with either PBS ($n = 5$), PTX ($n = 4$) or CAPN2-MSN ($n = 4$). Two-tailed *p*-values for CDK4 and cleaved caspase-3 were calculated by unpaired *t*-test. Two-way ANOVA was used to compare tumor growth curves. Levels of significance: ns = not significant, *p < 0.05, ****p < 0.0001.
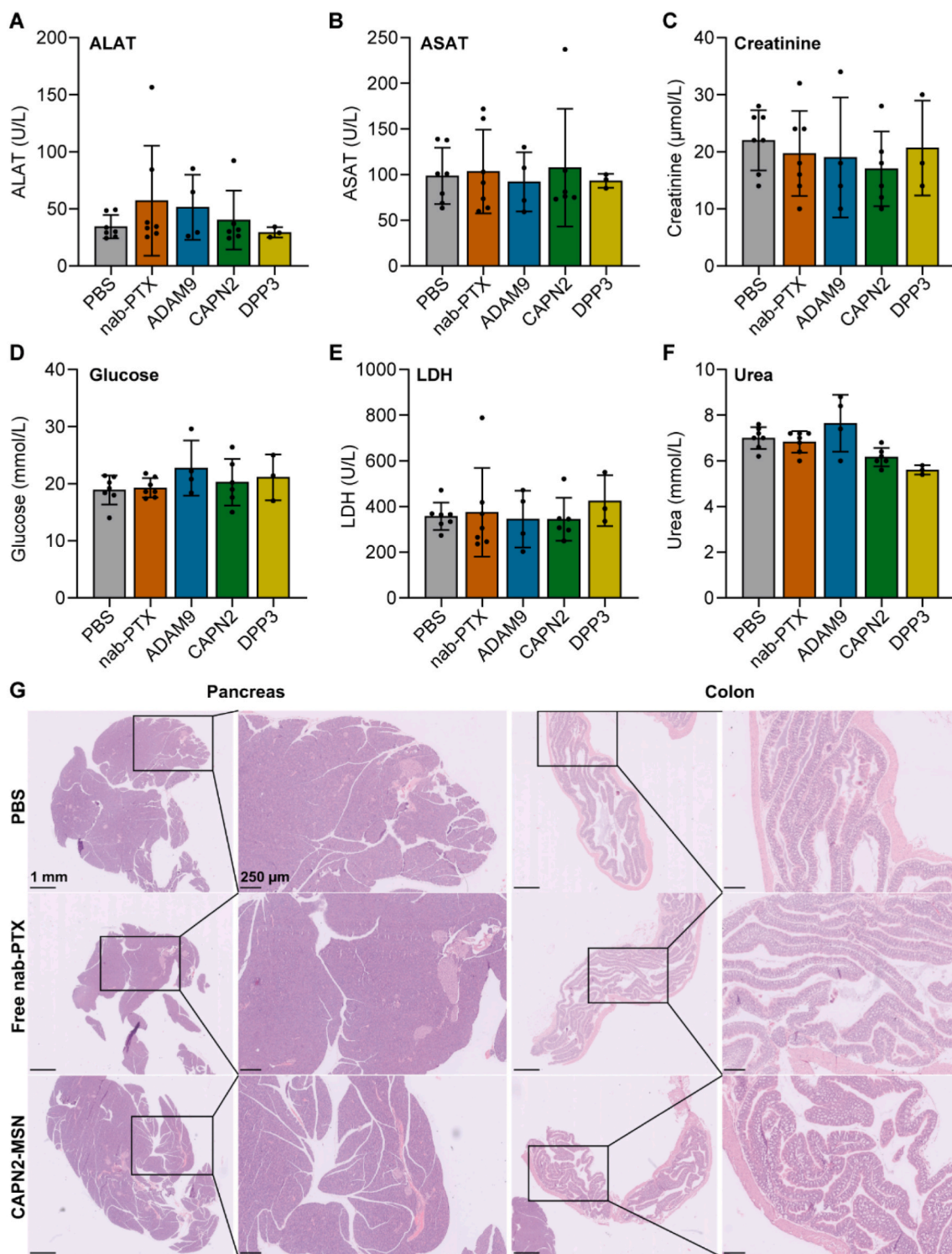
Fig. 6. Plasma ALAT (**A**), ALAT (**B**) and creatinine (**C**), glucose (**D**), LDH (**E**) and urea (**F**) levels in mice treated with for PBS ($n = 7$), nab-PTX ($n = 7$), ADAM9-MSN ($n = 4$), CAPN2-MSN ($n = 6$) and DPP3-MSN ($n = 3$) as measured by HPLC following standardized clinical guidelines of the AUMC. (**G**) H&E stained slides of the pancreas and colon of PBS, free nab-PTX and CAPN2-MSN treated mice.

cells are efficient in taking up the ADAM9-MSNs. Another explanation for the lack of antitumor efficacy could be that extracellularly deposited ADAM9 does not reach sufficient levels to cleave the ADAM9-MSNs in the abundance needed for the released paclitaxel to have a cytotoxic effect. A bioinformatic analysis revealed several promising intracellular candidates that exhibit heightened expression levels in PDAC relative to healthy pancreatic cells, with minimal expression in diverse healthy

blood cell populations and solid organs. Among these candidates, BACE2, CAPN2 and DPP3 stood out due to their reported peptide substrates in the existing literature [19–21]. BACE2 lacks organ-specific expression [33] and is involved in pigmentation [34], glucose homeostasis [35] and Alzheimer's disease [36]. More recently, BACE2 has been shown to be upregulated in a wide variety of cancer tissues and increased expression correlates with poor survival [37]. CAPN2 is a

Ca^{2+}-dependent cysteine protease and is involved in a wide variety of cellular processes and therefore plays a multifaceted role in human health [38]. The involvement of CAPN2 in many types of cancer has been long reported [39], and functional roles are reported in cell migration, invasion and chemosensitivity [40–42]. Therefore CAPN2 has been posed as an interesting therapeutic target [38]. DPP3 is an aminopeptidase involved in peptide degradation, including angiotensin II and enkephalins [43], and is therefore important for the regulation of blood pressure [44]. Other DPP3-mediated processes include inflammation, pain signaling and oxidative stress [44]. Aberrant DPP3 expression has been reported in a wide variety of cancers and is linked to poor survival [45]. The fact that all three candidates are well-known cancer-associated proteases validates the bioinformatic analysis and poses all three proteases as interesting candidates for the targeted delivery of chemotherapeutics.

Unexpectedly, treating PDAC cells with paclitaxel-loaded BACE2-MSNs did not mirror the toxicity profiles exhibited by CAPN2- and DPP3-MSNs. Only by increasing the concentration 4-fold an increase in cytotoxicity was observed, remarkably, however, increasing the concentration to 16-fold did not cause any additional toxicity. As negative surface charge may influence cellular uptake [46,47], the negative surface charge of BACE2-MSNs (Table 3) may have hampered cellular uptake with subsequent reduced cytotoxic activity. However, the limited toxicity can more likely be explained by the fact that BACE2 shows low levels of cleavage kinetics for multiple substrates [19,48], which includes the peptide linker employed in BACE2-MSN. Indeed, FRET-peptide cleavage experiments revealed poor cleavage kinetics of BACE2-substrate by PANC-1 cells (Supplemental Fig. 8). The lack of toxicity by BACE2-MSNs further reinforces our notion that PDAC cell death is caused by specific protease-mediated drug release. We have previously shown that slight alterations of the ADAM9-MSNs linker into an uncleavable-ADAM9-MSN did not result in cell death [13], with BACE2-MSN we demonstrate that not any type of linker can be employed and that drug release is linker and protease specific.

Next, we explored the degree of off-target cap removal and subsequent drug release by incubating neuronal and bone marrow-derived leukocytes with CAPN2- and DPP3-MSNs. No toxicity was observed except in neuronal cells upon incubation with the highest concentration of CAPN2-MSNs. The neuroblastoma origin of SH-SY5Y cells, widely used for studying neuronal function and differentiation [49], could account for this observed toxicity as CAPN2 overexpression is reported in a wide range of cancers [50–54]. This hypothesis is strengthened by the implication that CAPN2 is also involved in promoting malignant phenotypes in neuroblastoma [55].

Although both CAPN2- and DPP3-MSNs showed a reduction of side effects, a difference in antitumor effect could be observed in a subcutaneous KP2 PDAC model. It is challenging to explain the absence of antitumor efficacy by DPP3-MSNs, however, as the effect of free paclitaxel was already limited, we hypothesize that the amount of paclitaxel released from the DPP3-MSNs might have been insufficient to induce cell death. This explanation is supported by the observation that CAPN2-MSNs did cause cell death and that CAPN2 gene expression (Supplemental Fig. 9) and protein levels (Supplemental Fig. 10) are significantly higher in PDAC tissue compared to DPP3 expression. Next to differences in gene and protein expression levels, protease cleavage kinetics of the substrate (i.e. peptide linker) is an important factor driving drug release and subsequent cytotoxicity. Assessment of protease cleavage kinetics using FRET-peptides showed that CAPN2 cleavage kinetics were superior over DPP3 (Supplemental Fig. 8) further suggesting that *in vivo* drug release is more efficient from CAPN2-MSNS than form DPP3-MSNs explaining the superior anti-tumor activity of CAPN2-MSNs *in vivo*. Furthermore, as the DPP3-responsive linker is developed around the renin-angiotensin system [21] and implicated in kidney function [56, 57], the absence of kidney damage, as shown by unchanged creatinine and urea levels in the blood plasma, might indicate the general inability of cap removal of DPP3-MSNs under dynamic conditions. Additionally,

recent work showed the presence of DPP3 in extracellular fluids [43,58] and cell culture medium [59], possibly lowering the intracellular concentration of DPP3. Together, we thus hypothesize that all these factors might have hampered the efficacy of DPP3-MSNs *in vivo*. Importantly however, we cannot formally exclude that differences in bio-distribution between CAPN2- and DPP3-MSNs may –at least in part-explain the observed differences in anti-tumor activity. Irrespective the explanation for the observed differences in anti-tumor effects between CAPN2-MSNs and DPP3-MSNs *in vivo*, we did identify CAPN2-MSNs as an efficient and safe alternative to free drug delivery.

Replication of the subcutaneous model with PANC-1 cells in a NOD-scid IL2rγnull (NSG) mouse model yielded similar results. Promisingly, however, the antitumor efficacy of CAPN2-MSNs was even more pronounced. The increased clinical relevance can be explained by the heightened sensitivity of PANC-1 cells to CAPN2-MSNs compared to KP2 cells (Fig. 3B and 4A). This might not be so surprising as the identification of PDAC-enriched proteases was performed on human tissue and KP2 cells are of murine origin. No treatment group resulted in organ damage as demonstrated by analysis of blood plasma markers, confirming the safety of CAPN2-MSNs. The aforementioned overexpression of CAPN2 in a wide variety of cancers implies the broader applicability of the nano platform presented here.

While this study provides a promising alternative for the treatment of PDAC, it is important to acknowledge its limitations and potential drawbacks to ensure a comprehensive understanding of the research findings. The absence of *in vitro* (BACE2-MSN) and *in vivo* (DPP3-MSN) efficacy underscores the importance of the sensitivity and specificity of linker peptides incorporated onto the MSNs. The identification of protease substrates with increased sensitivity and specificity might improve preclinical efficacy and improve the chance of success of clinical implementation. One advantage of MSNs is the possibility of inner core and outer surface modifications. In this paper, we report rather 'basic' MSNs, lacking moieties that improve the targeted delivery, tumor penetration and cellular uptake. Equipping CAPN2-MSNs with such refinements might further improve clinical efficacy.

5. Conclusion

We present CAPN2-responsive MSNs as a promising therapeutic strategy for the treatment of PDAC. To harbor the efficient cellular uptake of MSNs by PDAC cells, as presented in this work, we identified several PDAC-enriched *intracellular* proteases and developed corresponding MSNs. Treatment of PDAC cells with paclitaxel-loaded MSNs responsive to CAPN2 and DPP3 resulted in efficient cell death. Two clinically relevant *in vitro* models showed a reduction of common paclitaxel-induced side effects upon MSNs administration as compared to free paclitaxel, confirming PDAC-specificity. Finally, we show that treatment with CAPN2-responsive MSNs has superior antitumor efficacy as compared to systemic paclitaxel administration *in vivo*, without resulting in severe adverse effects.

Institutional review board statement

The study was conducted in accordance with the Declaration of Helsinki, and approved by the Institutional Animal Care and Use Committee of the AUMC according to protocol DIX-19-9064.

Data availability statement

The data presented in this study are available from the corresponding author upon reasonable request.

CRediT authorship contribution statement

Etienne J. Slapak: Writing – review & editing, Writing – original draft, Visualization, Validation, Project administration, Methodology, Investigation, Formal analysis, Data curation, Conceptualization. **Mouad el Mandili:** Writing – review & editing, Validation, Methodology, Investigation, Formal analysis. **Marieke S. Ten Brink:** Investigation. **Alexander Kros:** Writing – review & editing, Supervision, Resources. **Maarten F. Bijlsma:** Conceptualization, Project administration, Resources, Supervision, Writing – review & editing. **C. Arnold Spek:** Writing – review & editing, Writing – original draft, Supervision, Resources, Project administration, Conceptualization, Funding acquisition.

Declaration of competing interest

The authors declare that they have no known competing financial interests or personal relationships that could have appeared to influence the work reported in this paper.

Acknowledgements

Appendix A. Supplementary data

Supplementary data to this article can be found online at https://doi.org/10.1016/j.canlet.2024.216845.

References

[1] R.L. Siegel, K.D. Miller, H.E. Fuchs, A. Jemal, Cancer statistics, 2021, CA Cancer J Clin 71 (2021) 7–33, https://doi.org/10.3322/caac.21654.

[2] J.D. Mizrahi, R. Surana, J.W. Valle, R.T. Shroff, Pancreatic cancer, Lancet 395 (2020) 2008–2020, https://doi.org/10.1016/s0140-6736(20)30974-0.

[3] A. McBride, M. Bonafede, Q. Cai, N. Princic, O. Tran, C. Pelletier, M. Parisi, M. Patel, Comparison of treatment patterns and economic outcomes among metastatic pancreatic cancer patients initiated on nab-paclitaxel plus gemcitabine versus FOLFIRINOX, Expet Rev. Clin. Pharmacol. 10 (2017) 1153–1160, https://doi.org/10.1080/17512433.2017.1365598.

[4] F.U. Din, W. Aman, I. Ullah, O.S. Qureshi, O. Mustapha, S. Shafique, A. Zeb, Effective use of nanocarriers as drug delivery systems for the treatment of selected tumors, Int. J. Nanomed. 12 (2017) 7291–7309, https://doi.org/10.2147/ijn.S146315.

[5] E.J. Slapak, M. El Mandili, M.F. Bijlsma, C.A. Spek, Mesoporous silica nanoparticle-based drug delivery systems for the treatment of pancreatic cancer: a systematic literature overview, Pharmaceutics 14 (2022), https://doi.org/10.3390/pharmaceutics14020390.

[6] A. Watermann, J. Brieger, Mesoporous silica nanoparticles as drug delivery vehicles in cancer, Nanomaterials 7 (2017), https://doi.org/10.3390/nano7070189.

[7] F. Porta, G.E.M. Lamers, J.I. Zink, A. Kros, Peptide modified mesoporous silica nanocontainers, Phys. Chem. Chem. Phys. 13 (2011) 9982–9985, https://doi.org/10.1039/C0CP02959A.

[8] F. Porta, G.E. Lamers, J. Morrhayim, A. Chatzopoulou, M. Schaaf, H. den Dulk, C. Backendorf, J.I. Zink, A. Kros, Folic acid-modified mesoporous silica nanoparticles for cellular and nuclear targeted drug delivery, Adv. Healthcare Mater. 2 (2013) 281–286, https://doi.org/10.1002/adhm.201200176.

[9] J. Lu, M. Liong, Z. Li, J.I. Zink, F. Tamanoi, Biocompatibility, biodistribution, and drug-delivery efficiency of mesoporous silica nanoparticles for cancer therapy in animals, Small 6 (2010) 1794–1805, https://doi.org/10.1002/smll.201000538.

[10] E.J. Slapak, J. Duitman, C. Tekin, M.F. Bijlsma, C.A. Spek, Matrix metalloproteases in pancreatic ductal adenocarcinoma: key drivers of disease progression? Biology 9 (2020) 80, https://doi.org/10.3390/biology9040080.

[11] E.J. Slapak, L. Kong, M. El Mandili, R. Nieuwland, A. Kros, M.F. Bijlsma, C.A. Spek, ADAM9-Responsive mesoporous silica nanoparticles for targeted drug delivery in pancreatic cancer, Cancers 13 (2021), https://doi.org/10.3390/cancers13133321.

[12] N. Singh, A. Saraya, Roles of cathepsins in pancreatic cancer, Trop. Gastroenterol. 37 (2016) 77–85.

[13] E.J. Slapak, M. el Mandili, M.S.T. Brink, A. Kros, M.F. Bijlsma, C.A. Spek, Preclinical assessment of ADAM9-responsive mesoporous silica nanoparticles for the treatment of pancreatic cancer, Int. J. Mol. Sci. 24 (2023) 10704.

[14] T. Wang, Y. Liu, C. Wu, Effect of paclitaxel-mesoporous silica nanoparticles with a core-shell structure on the human lung cancer cell line A549, Nanoscale Res. Lett. 12 (2017) 66, https://doi.org/10.1186/s11671-017-1826-1.

[15] P. Bankhead, M.B. Loughrey, J.A. Fernández, Y. Dombrowski, D.G. McArt, P.D. Dunne, S. McQuaid, R.T. Gray, L.J. Murray, H.G. Coleman, et al., QuPath: open source software for digital pathology image analysis, Sci. Rep. 7 (2017) 16878, https://doi.org/10.1038/s41598-017-17204-5.

[16] C.W. Chou, Y.K. Huang, T.T. Kuo, J.P. Liu, Y.P. Sher, An overview of ADAM9: structure, activation, and regulation in human diseases, Int. J. Mol. Sci. 21 (2020) 1–22, https://doi.org/10.3390/ijms21207790.

[17] R. Kappelhoff, X.S. Puente, C.H. Wilson, A. Seth, C. López-Otín, C.M. Overall, Overview of transcriptomic analysis of all human proteases, non-proteolytic homologs and inhibitors: organ, tissue and ovarian cancer cell line expression profiling of the human protease degradome by the CLIP-CHIP™ DNA microarray, Biochim. Biophys. Acta Mol. Cell Res. 1864 (2017) 2210–2219, https://doi.org/10.1016/j.bbamcr.2017.08.004.

[18] D.T. Lin, E. Conibear, ABHD17 proteins are novel protein depalmitoylases that regulate N-Ras palmitate turnover and subcellular localization, Elife 4 (2015) e11306, https://doi.org/10.7554/eLife.11306.

[19] F. Grüninger-Leitch, D. Schlatter, E. Küng, P. Nelböck, H. Döbeli, Substrate and inhibitor profile of BACE (beta-secretase) and comparison with other mammalian aspartic proteases, J. Biol. Chem. 277 (2002) 4687–4693, https://doi.org/10.1074/jbc.M109266200.

[20] C.E. McCartney, J.A. MacLeod, P.A. Greer, P.L. Davies, An easy-to-use FRET protein substrate to detect calpain cleavage in vitro and in vivo, Biochim. Biophys. Acta Mol. Cell Res. 1865 (2018) 221–230, https://doi.org/10.1016/j.bbamcr.2017.10.013.

[21] S.C. Prajapati, S.S. Chauhan, Dipeptidyl peptidase III: a multifaceted oligopeptide N-end cutter, FEBS J. 278 (2011) 3256–3276, https://doi.org/10.1111/j.1742-4658.2011.08275.x.

[22] M.J. Garnett, E.J. Edelman, S.J. Heidorn, C.D. Greenman, A. Dastur, K.W. Lau, P. Greninger, I.R. Thompson, X. Luo, J. Soares, et al., Systematic identification of genomic markers of drug sensitivity in cancer cells, Nature 483 (2012) 570–575, https://doi.org/10.1038/nature11005.

[23] J. Barretina, G. Caponigro, N. Stransky, K. Venkatesan, A.A. Margolin, S. Kim, C.J. Wilson, J. Lehár, G.V. Kryukov, D. Sonkin, et al., The Cancer Cell Line Encyclopedia enables predictive modelling of anticancer drug sensitivity, Nature 483 (2012) 603–607, https://doi.org/10.1038/nature11003.

[24] T. Idichi, N. Seki, H. Kurahara, Y. Yonemori, Y. Osako, T. Arai, A. Okato, Y. Kita, T. Arigami, Y. Mataki, et al., Regulation of actin-binding protein ANLN by antitumor miR-217 inhibits cancer cell aggressiveness in pancreatic ductal adenocarcinoma, Oncotarget 8 (2017) 53180–53193, https://doi.org/10.18632/oncotarget.18261.

[25] S. Yang, P. He, J. Wang, A. Schetter, W. Tang, N. Funamizu, K. Yanaga, T. Uwagawa, A.R. Satoskar, J. Gaedcke, et al., A novel MIF signaling pathway drives the malignant character of pancreatic cancer by targeting NR3C2, Cancer Res. 76 (2016) 3838–3850, https://doi.org/10.1158/0008-5472.Can-15-2841.

[26] K.A. Ellsworth, B.W. Eckloff, L. Li, I. Moon, B.L. Fridley, G.D. Jenkins, E. Carlson, A. Brisbin, R. Abo, W. Bamlet, et al., Contribution of FKBP5 genetic variation to gemcitabine treatment and survival in pancreatic adenocarcinoma, PLoS One 8 (2013) e70216, https://doi.org/10.1371/journal.pone.0070216.

[27] T.R. Donahue, L.M. Tran, R. Hill, Y. Li, A. Kovochich, J.H. Calvopina, S.G. Patel, N. Wu, A. Hindoyan, J.J. Farrell, et al., Integrative survival-based molecular profiling of human pancreatic cancer, Clin. Cancer Res. 18 (2012) 1352–1363, https://doi.org/10.1158/1078-0432.Ccr-11-1539.

[28] N. Novershtern, A. Subramanian, L.N. Lawton, R.H. Mak, W.N. Haining, M.E. McConkey, N. Habib, N. Yosef, C.Y. Chang, T. Shay, et al., Densely interconnected transcriptional circuits control cell states in human hematopoiesis, Cell 144 (2011) 296–309, https://doi.org/10.1016/j.cell.2011.01.004.

[29] A.R. Abbas, D. Baldwin, Y. Ma, W. Ouyang, A. Gurney, F. Martin, S. Fong, M. van Lookeren Campagne, P. Godowski, P.M. Williams, et al., Immune response in silico (IRIS): immune-specific genes identified from a compendium of microarray expression data, Gene Immun. 6 (2005) 319–331, https://doi.org/10.1038/sj.gene.6364173.

[30] Y.J. Heng, C.E. Pennell, H.N. Chua, J.E. Perkins, S.J. Lye, Whole blood gene expression profile associated with spontaneous preterm birth in women with threatened preterm labor, PLoS One 9 (2014) e96901, https://doi.org/10.1371/journal.pone.0096901.

[31] P.G. Woodruff, L.L. Koth, Y.H. Yang, M.W. Rodriguez, S. Favoreto, G.M. Dolganov, A.C. Paquet, D.J. Erle, A distinctive alveolar macrophage activation state induced by cigarette smoking, Am. J. Respir. Crit. Care Med. 172 (2005) 1383–1392, https://doi.org/10.1164/rccm.200505-686OC.

[32] S.C. Kim, D.W. Kim, Y.H. Shim, J.S. Bang, H.S. Oh, S. Wan Kim, M.H. Seo, In vivo evaluation of polymeric micellar paclitaxel formulation: toxicity and efficacy,

J. Contr. Release 72 (2001) 191–202, https://doi.org/10.1016/s0168-3659(01)00275-9.

[33] B.D. Bennett, S. Babu-Khan, R. Loeloff, J.C. Louis, E. Curran, M. Citron, R. Vassar, Expression analysis of BACE2 in brain and peripheral tissues, J. Biol. Chem. 275 (2000) 20647–20651, https://doi.org/10.1074/jbc.M002688200.

[34] L. Rochin, I. Hurbain, L. Serneels, C. Fort, B. Watt, P. Leblanc, M.S. Marks, B. De Strooper, G. Raposo, G. van Niel, BACE2 processes PMEL to form the melanosome amyloid matrix in pigment cells, Proc Natl Acad Sci U S A 110 (2013) 10658–10663, https://doi.org/10.1073/pnas.1220748110.

[35] D. Esterházy, I. Stützer, H. Wang, M.P. Rechsteiner, J. Beauchamp, H. Döbeli, H. Hilpert, H. Matile, H. Prummer, A. Schmidt, et al., Bace2 is a β cell-enriched protease that regulates pancreatic β cell function and mass, Cell Metabol. 14 (2011) 365–377, https://doi.org/10.1016/j.cmet.2011.06.018.

[36] Z. Wang, Q. Xu, F. Cai, X. Liu, Y. Wu, W. Song, BACE2, a conditional β-secretase, contributes to Alzheimer's disease pathogenesis, JCI Insight 4 (2019), https://doi.org/10.1172/jci.insight.123431.

[37] F. Farris, V. Matafora, A. Bachi, The emerging role of β-secretases in cancer, J. Exp. Clin. Cancer Res. 40 (2021) 147, https://doi.org/10.1186/s13046-021-01953-3.

[38] I. Shapovalov, D. Harper, P.A. Greer, Calpain as a therapeutic target in cancer, Expert Opin. Ther. Targets 26 (2022) 217–231, https://doi.org/10.1080/14728222.2022.2047178.

[39] S.J. Storr, N.O. Carragher, M.C. Frame, T. Parr, S.G. Martin, The calpain system and cancer, Nat. Rev. Cancer 11 (2011) 364–374, https://doi.org/10.1038/nrc3050.

[40] S.J. Franco, A. Huttenlocher, Regulating cell migration: calpains make the cut, J. Cell Sci. 118 (2005) 3829–3838, https://doi.org/10.1242/jcs.02562.

[41] S. Grieve, Y. Gao, C. Hall, J. Hu, P.A. Greer, Calpain genetic disruption and HSP90 inhibition combine to attenuate mammary tumorigenesis, Mol. Cell Biol. 36 (2016) 2078–2088, https://doi.org/10.1128/mcb.01062-15.

[42] J.A. MacLeod, Y. Gao, C. Hall, W.J. Muller, T.S. Gujral, P.A. Greer, Genetic disruption of calpain-1 and calpain-2 attenuates tumorigenesis in mouse models of HER2+ breast cancer and sensitizes cancer cells to doxorubicin and lapatinib, Oncotarget 9 (2018) 33382–33395, https://doi.org/10.18632/oncotarget.26078.

[43] P. Kaufmann, M. Muenzner, M. Kästorf, K. Santos, T. Hartmann, A. Dienelt, L. Rehfeld, A. Bergmann, A novel and highly efficient purification procedure for native human dipeptidyl peptidase 3 from human blood cell lysate, PLoS One 14 (2019) e0220866, https://doi.org/10.1371/journal.pone.0220866.

[44] P. Ye, W. Duan, Y.Q. Leng, Y.K. Wang, X. Tan, W.Z. Wang, DPP3: from biomarker to therapeutic target of cardiovascular diseases, Front Cardiovasc Med 9 (2022) 974035, https://doi.org/10.3389/fcvm.2022.974035.

[45] G. Malovan, B. Hierzberger, S. Suraci, M. Schaefer, K. Santos, S. Jha, P. Macheroux, The emerging role of dipeptidyl peptidase 3 in pathophysiology, FEBS J. 290 (2023) 2246–2262, https://doi.org/10.1111/febs.16429.

[46] T.-H. Chung, S.-H. Wu, M. Yao, C.-W. Lu, Y.-S. Lin, Y. Hung, C.-Y. Mou, Y.-C. Chen, D.-M. Huang, The effect of surface charge on the uptake and biological function of mesoporous silica nanoparticles in 3T3-L1 cells and human mesenchymal stem cells, Biomaterials 28 (2007) 2959–2966, https://doi.org/10.1016/j.biomaterials.2007.03.006.

[47] I. Slowing, B.G. Trewyn, V.S.Y. Lin, Effect of surface functionalization of MCM-41-type mesoporous silica nanoparticles on the endocytosis by human cancer cells, J. Am. Chem. Soc. 128 (2006) 14792–14793, https://doi.org/10.1021/ja0645943.

[48] I. Voytyuk, S.A. Mueller, J. Herber, A. Snellinx, D. Moechars, G. van Loo, S. F. Lichtenthaler, B. De Strooper, BACE2 distribution in major brain cell types and identification of novel substrates, Life Sci. Alliance 1 (2018) e201800026, https://doi.org/10.26508/lsa.201800026.

[49] J.I. Forster, S. Köglsberger, C. Trefois, O. Boyd, A.S. Baumuratov, L. Buck, R. Balling, P.M. Antony, Characterization of differentiated SH-SY5Y as neuronal screening model reveals increased oxidative vulnerability, J. Biomol. Screen 21 (2016) 496–509, https://doi.org/10.1177/1087057115625190.

[50] X.-L. Ma, K.-Y. Zhu, Y.-D. Chen, W.-G. Tang, S.-H. Xie, H. Zheng, Y. Tong, Y.-C. Wang, N. Ren, L. Guo, et al., Identification of a novel Calpain-2-SRC feed-back loop as necessity for β-Catenin accumulation and signaling activation in hepatocellular carcinoma, Oncogene 41 (2022) 3554–3569, https://doi.org/10.1038/s41388-022-02367-x.

[51] W.-c. Ho, L. Pikor, Y. Gao, B.E. Elliott, P.A. Greer, Calpain 2 regulates akt-FoxO-p27Kip1 protein signaling pathway in mammary carcinoma, J. Biol. Chem. 287 (2012) 15458–15465, https://doi.org/10.1074/jbc.M112.349308.

[52] C. Miao, C. Liang, Y. Tian, A. Xu, J. Zhu, K. Zhao, J. Zhang, Y. Hua, S. Liu, H. Dong, et al., Overexpression of CAPN2 promotes cell metastasis and proliferation via AKT/mTOR signaling in renal cell carcinoma, Oncotarget 8 (2017), https://doi.org/10.18632/oncotarget.22083.

[53] S.J. Storr, S. Safuan, C.M. Woolston, T. Abdel-Fatah, S. Deen, S.Y. Chan, S. G. Martin, Calpain-2 expression is associated with response to platinum based chemotherapy, progression-free and overall survival in ovarian cancer, J. Cell Mol. Med. 16 (2012) 2422–2428, https://doi.org/10.1111/j.1582-4934.2012.01559.x.

[54] P. Li, C. Miao, C. Liang, P. Shao, Z. Wang, J. Li, Silencing CAPN2 expression inhibited castration-resistant prostate cancer cells proliferation and invasion via AKT/mTOR signal pathway, BioMed Res. Int. 2017 (2017) 2593674, https://doi.org/10.1155/2017/2593674.

[55] W.J. Lee, C.H. Shin, H. Ji, S.D. Jeong, M.S. Park, H.H. Won, P.R. Pandey, D. Tsitsipatis, M. Gorospe, H.H. Kim, hnRNPK-regulated LINC00263 promotes malignant phenotypes through miR-147a/CAPN2, Cell Death Dis. 12 (2021) 290, https://doi.org/10.1038/s41419-021-03575-1.

[56] X. Pang, A. Shimizu, S. Kurita, D.P. Zankov, K. Takeuchi, M. Yasuda-Yamahara, S. Kume, T. Ishida, H. Ogita, Novel therapeutic role for dipeptidyl peptidase III in the treatment of hypertension, Hypertension 68 (2016) 630–641, https://doi.org/10.1161/hypertensionaha.116.07357.

[57] S. Jha, U. Taschler, O. Domenig, M. Poglitsch, B. Bourgeois, M. Pollheimer, L. M. Pusch, G. Malovan, S. Frank, T. Madl, et al., Dipeptidyl peptidase 3 modulates the renin-angiotensin system in mice, J. Biol. Chem. 295 (2020) 13711–13723, https://doi.org/10.1074/jbc.RA120.014183.

[58] H. Sato, K. Kimura, Y. Yamamoto, T. Hazato, [Activity of DPP III in human cerebrospinal fluid derived from patients with pain], Masui 52 (2003) 257–263.

[59] N. Cruz-Diaz, B.A. Wilson, N.T. Pirro, K.B. Brosnihan, A.C. Marshall, M. C. Chappell, Identification of dipeptidyl peptidase 3 as the Angiotensin-(1-7) degrading peptidase in human HK-2 renal epithelial cells, Peptides 83 (2016) 29–37, https://doi.org/10.1016/j.peptides.2016.06.005.